

A Lossy Counting-Based State of Charge Estimation Method and Its Application to Electric Vehicles

Hong Zhang ¹, Li Zhao ^{1,2,*} and Yong Chen ^{2,3}

Received: 13 May 2015; Accepted: 25 November 2015; Published: 4 December 2015

Academic Editor: Omar Hegazy

¹ School of Mechanical and Vehicular Engineering, Beijing Institute of Technology, Beijing 100081, China; zhanghong@bit.edu.cn

² Collaborative Innovation Center of Electric Vehicles in Beijing, Beijing 100192, China; chen Yong_jz@126.com

³ Mechanical Electrical Engineering School, Beijing Information Science & Technology University, Beijing 100192, China

* Correspondence: zhaoli@bit.edu.cn; Tel.: +86-156-3230-4969 or +86-10-6894-0589

Abstract: Estimating the residual capacity or state-of-charge (SoC) of commercial batteries on-line without destroying them or interrupting the power supply, is quite a challenging task for electric vehicle (EV) designers. Many Coulomb counting-based methods have been used to calculate the remaining capacity in EV batteries or other portable devices. The main disadvantages of these methods are the cumulative error and the time-varying Coulombic efficiency, which are greatly influenced by the operating state (SoC, temperature and current). To deal with this problem, we propose a lossy counting-based Coulomb counting method for estimating the available capacity or SoC. The initial capacity of the tested battery is obtained from the open circuit voltage (OCV). The charging/discharging efficiencies, used for compensating the Coulombic losses, are calculated by the lossy counting-based method. The measurement drift, resulting from the current sensor, is amended with the distorted Coulombic efficiency matrix. Simulations and experimental results show that the proposed method is both effective and convenient.

Keywords: battery management systems (BMS); state of charge (SoC); Coulombic efficiency; lossy counting method (LC)

1. Introduction

State-of-charge (SoC) estimation is an important issue in the lithium-ion battery area. Without such an estimation system, it is very difficult to avoid the unpredicted-system-interruptions for EVs, and the cells in a pack are easily over-charged and over-discharged [1–3]. This will result in permanent damage to the internal structure of the cells. Several methods have been used to estimate the SoC in electrical chemistry laboratories and their accuracy has been verified [4–6]. However, estimating the SoC of commercial batteries on-line without destroying them or interrupting the battery power supply is still quite a challenging task for electric vehicle (EV) designers.

The discharge test method is a reliable method to determine the SoC of batteries and the remaining charge can be precisely calculated with it [7–9]. However, the time consumed for the testing is very long and after the test, no power is left in the battery, so, it is not appropriate for on-line estimation. The open circuit voltage (OCV) method is another frequently-used method for SoC calibration. Its fundamental principle is that SoC has a special relationship with the embedded quantity of lithium-ion in the active material and there is a one-to-one correspondence between SoC and OCV [10,11]. Thus, after adequate resting, the SoC of a battery can be estimated by the open

circuit voltage. However, the state-switching (from an operating state to a balanced state) will take up a very long time and its duration is tied to the state of SoC, temperature, and so on, so the OCV method cannot be used for EVs in driving status. To deal with this problem, researchers have developed several model-based SoC estimation methods, in which precise and complex battery models (the combining model, the Rint model, the ESC mode, *etc.*) were used for estimating the battery capacity [12–14]. With the proposed models, the SoC of batteries can be dynamic estimated on-line. The estimation precisions are largely decided by the models and the collected signals. Many research results demonstrate that the first-order RC model with one-state hysteresis is suitable for LiFePO₄ batteries [15], but the expensive computational cost makes them unsuitable for EVs with limited calculation resources. In addition, the neural network model method is a nonlinear estimation method, which does not take into account the details of the batteries [16,17]. Thus, it is suitable to be used for estimating different kinds of batteries. The drawback of this method is that it needs a great number of training samples and lengthy training procedures.

In practice, many SoC estimation methods have been proposed and most of them estimate the battery state with indirect parameters [18]. For example, terminal voltage and internal resistance are frequently-used parameters for SoC estimation. However, these parameters always change irregularly when an EV is running in real-life condition. Furthermore, the state-of-health (SoH) of a battery has a huge impact on these parameters [19,20]. Thus, the SoC estimation methods, relying on these indirect parameters, can hardly obtain precise estimation results.

On the contrary, the Coulomb counting method calculates the remaining capacity by accumulating the amount of the direct parameter—current [21,22]. This is a simple and general method, and its precision is defined mainly by the sampling precision and the frequency of the current sensor. Nowadays, many portable devices and electric vehicles, equipped with computable hardware and large memory size, can estimate the remaining battery capacities using this method [23]. As an open loop SoC estimation method, the errors of the Coulomb counting method are accumulated in the current integral process. As the detection time increases, the cumulative error increases accordingly [24,25]. The estimation result is greatly influenced by the precision of the current sensor and the measurement drift, which will result in cumulative effects [26,27]. Additionally, the Coulomb counter does not take into account the age and capacity-changes of the battery. Thus, the disadvantages of this method hinder its further application [28]. For example, the Coulombic efficiency is greatly influenced by the operating status of the battery (SoC, temperature and current) and this is difficult to measure [29–32].

To deal with this problem, we propose a lossy counting-based relative Coulomb counting method for estimating the available capacity or SoC of lithium-ion batteries. The initial capacity of the tested battery is obtained with the OCV-SoC curve. The charging/discharging efficiencies, used for compensating the Coulombic losses, are dynamically corrected by a lossy counting method. The measurement drift, coming from the current sensor, is amended with a relative accumulating manner of charge.

The rest of this paper is organized as follows: we first reviewed the related work on the lossy counting method (LC). Secondly, we present the LC-based SoC or available capacity estimation method for lithium-ion batteries. Then we describe several experiments, in which different parameters of the algorithm are examined. With these experiments, we demonstrated how to accumulate the summary information and to calculate the SoC or available capacity for the proposed algorithm. Finally, we concluded this paper by highlighting the key contributions of this work.

2. Related Work

2.1. Lossy Counting Method

A data stream is an ordered sequence of instances. Data stream mining is the process of extracting knowledge from rapid or continuous data records [33,34]. In many applications, such as computer network traffic, phone conversations, ATM transactions, web searches and sensor data, the

given data stream can be read only once or the time used for computation or storage is very short. Many concepts used in data stream mining come from incremental learning (IL). Many incremental heuristic search algorithms are used to cope with the structural changes and online learning demands.

Lossy counting is a deterministic algorithm, which calculates frequency counts over a stream of single item transactions [35]. It can satisfy some special guarantees (for example, some static thresholds) using at most $(\log(\epsilon \times N))/\epsilon$ space, where N denotes the current length of the data stream. Two special parameters, support s and error ϵ , should be specified by the user.

Definitions: The received data stream is divided into buckets and each bucket has $w = 1/\epsilon$ transactions. The buckets are labeled with bucket ids, starting from 1. The current bucket id is $b_{current}$, the value of which is N/w . For an element e , the true frequency of it in the data stream (from the starting point to the current recorder) is f_e . In these parameters, N , $b_{current}$ and f_e are variables, the values of which change with the stream progresses. ϵ and w are unchanged parameters, the value of which is fixed. To calculate the frequency, a data structure $D(e, f, \Delta)$ is given, where e is an element in the stream, f is the estimated frequency of the element e , and Δ is the maximum possible error in f .

Algorithm

- 1: Initialization. Empty D
- 2: Read in a newly arrived element e and lookup D to see whether or not an entry for e has existed. If it exists, update the entry by incrementing its frequency f by one. Otherwise, create a new entry of the form $(e, 1, b_{current}-1)$.
- 3: Boundary judging. When a bucket boundary arrived, prune D by deleting the entries in it and go (2). The rule for deletion is “for an entry (e, f, Δ) , if $f + \Delta \leq b_{current}$, then delete it”.

Whenever a user asks for the list of items with threshold s , the entries $(f \geq (s - \epsilon) \cdot N)$ will be output. This can be seen in Figure 1.

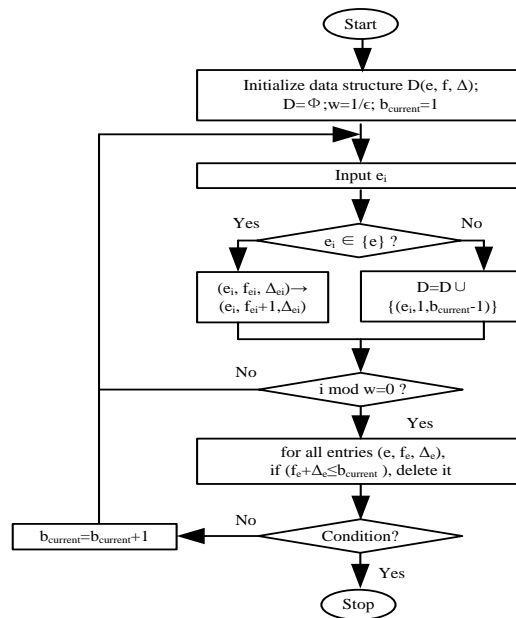


Figure 1. The flow chart of the lossy counting method.

2.2. Coulomb Counting Method

The Coulomb counting method (Ampere-hour integral method) is the most common and straightforward method for estimating battery SoC. Many battery management systems calculate SoC with the basic Coulomb counting method or its variations [22,26]. In these approaches, the current leaving and entering the battery is calculated periodically and the SoC of the battery is estimated by subtracting or adding the cumulative net charge.

Definition 1. (State of charge, SoC). Let C_N be the rated capacity of a battery, $SoC(t_0)$ be the SoC at the initial time t_0 , η be the coulombic efficiency, $I(t)$ be the current which is positive at discharge and negative at charge, with the measured current, the SoC obtained with Ampere-hour integral method could be represented by:

$$SoC(t) = SoC(t_0) - \frac{1}{C_N} \int_{t_0}^t \eta \times I(t) dt \quad (1)$$

Usually, the initial SoC, $SoC(t_0)$, can be estimated by the open-circuit voltage based approach or by the relationship between SoC and parameters in a standard charging stage. The rated capacity, C_N , can be obtained from the battery manufacturer or be measured in the laboratory. The precise current, $I(t)$, can be achieved by investing more money in the equipment measurement. However, the accurate Coulombic efficiency, η , cannot be simply estimated with common methods. In fact, the value of η keeps on changing during the whole discharging or charging process. Replacing the real values of η with an average value or an estimated one, is not a feasible way for estimating SoC. The charge or discharge current, temperature, SoC range, SoH and many other factors impose their influence on the Coulombic efficiency during the calculation processes.

2.3. Coulombic Efficiency (η)

Definition 2. (Average Coulombic efficiency, η). Let I_d be the discharge current, I_c be the charge current, t_d be the discharge time, t_c be the charge time, the coulombic efficiency of the test battery, η , could be represented by:

$$\eta = \int_0^{t_d} I_d dt / \int_0^{t_c} I_c dt \quad (2)$$

Definition 3. (Charge coulombic efficiency, η_{c,I_n}). Discharge a battery at $C/3$ rate until the cut off voltage is reached, and then, charge it at a specified current I_n until $SoC = 1$. The charged capacity is $Q_{c,I_n} = I_n \cdot t_{c,I_n}$, where t_{c,I_n} is the charge time. After 10 min rest, the battery was discharged at $C/3$ rate until its cut off voltage. The discharged capacity is $Q_{d,C/3} = (C/3)t_{d,C/3}$, where $t_{d,C/3}$ is the discharge time. Thus, the charge Coulombic efficiency can be calculated like this:

$$\eta_{c,I_n} = Q_{d,C/3} / Q_{c,I_n} = (C/3 t_{d,C/3}) / (I_n \times t_{c,I_n})$$

Definition 4. (Discharge coulombic efficiency, η_{d,I_n}). Discharge a battery with current I_n until the cut off voltage is reached, and then, charge it at $C/3$ rate until $SoC = 1$. The charged capacity is $Q_{c,C/3} = (C/3) \cdot t_{c,C/3}$, where $t_{c,C/3}$ is the charge time. After 10 min rest, discharge the battery at a current I_n until its cut off voltage. The discharged capacity is $Q_{d,I_n} = (I_n)t_{d,I_n}$, where t_{d,I_n} is the discharge time. Thus, the discharge Coulombic efficiency can be calculated like this:

$$\eta_{d,I_n} = Q_{d,I_n} / Q_{c,C/3} = (I_n \times t_{d,I_n}) / (C/3 t_{c,C/3})$$

In the charge/discharge process, battery energy losses are inevitable. Under laboratory conditions, the average Coulombic efficiency, η , can be calculated by Equation (2). However, in actual conditions, the charge and discharge process in EV keeps alternating and all of the factors (current,

temperature, and capacity) change continuously and sharply. It is hard to find an effective method or equipment to calculate the average Coulombic efficiency accurately. For example, the charge and discharge Coulombic efficiency of a given cell are shown in Figure 2a,b. The discharge Coulombic efficiencies of different temperatures and available capacities are shown in Figure 2c,d. The calculation method can be observed in [25]. From Figure 2a–d, we can see that the changing range of the Coulombic efficiency is very large. Without recording all of the detailed charge/discharge information, it is not possible to obtain an accurate SoC estimation.

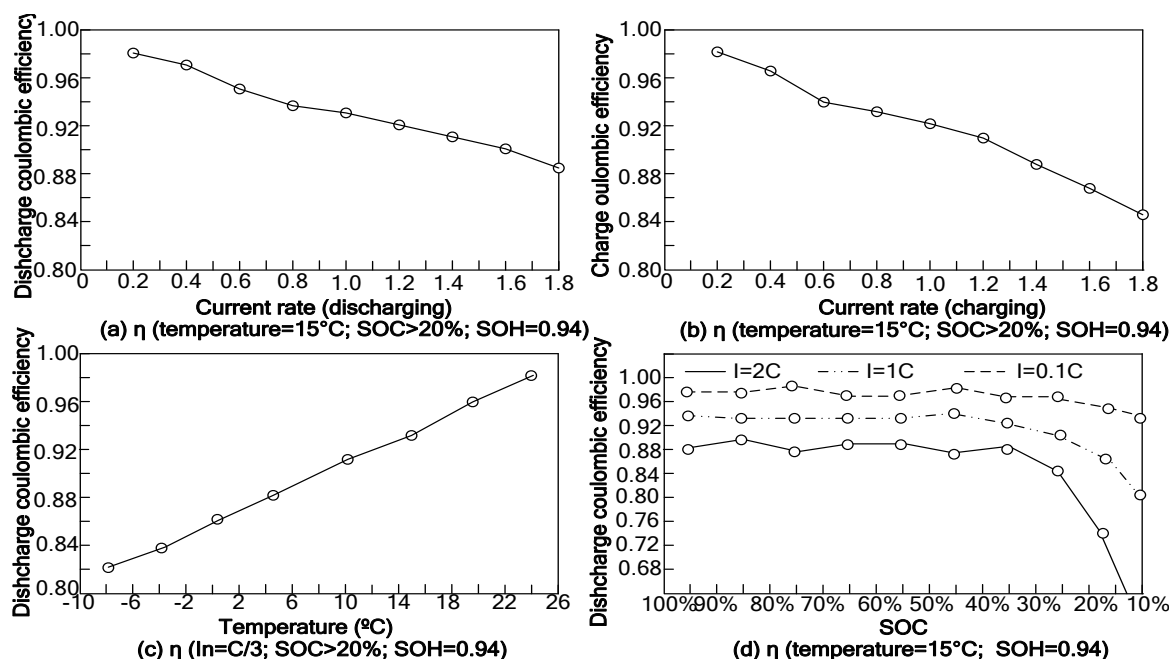


Figure 2. The influences of discharge/charge current, temperature and available capacity on Coulombic efficiency. (a) η (temperature = 15 °C, SoC > 20%, SoH = 0.94) for discharging; (b) η (temperature = 15 °C, SoC > 20%, SoH = 0.94) for charging; (c) η ($I_n = C/3$, SoC > 20%, SoH = 0.94); (d) η (temperature = 15 °C, SoH = 0.94).

3. LC-Based SoC Estimating Method

In fact, under actual driving conditions, it is very hard to accurately calculate the SoC or available capacity with the estimated Coulombic efficiency needed by Equation (1) during the whole charge or discharge process. Many factors have effects on the Coulombic efficiency and the calculation result. Thus, accumulating the measured current and correcting it with an accurate Coulombic efficiency at each measurement point perhaps is the only feasible way. Under such a condition, Equation (1) can be substituted by Equation (3), where $I(t)$, $T(t)$, $SoC(t)$, $SoH(t)$ are the current, temperature, SoC and SoH of the battery at time t :

$$SoC(t) = SoC(t_0) - \frac{1}{C_N} \int_{t_0}^t \eta_{[I(t), T(t), SoC(t), SoH(t)]} \times I(t) dt \tag{3}$$

In practice, the sensors can only send data at every discrete time point, t_k ($t_k = \Delta t \times k$). Δt is the sampling interval and k is the number of sampling. Thus, we can get:

$$SoC(t) \approx SoC(t_0) - \frac{1}{C_N} \times \sum_{t_k = \Delta t \times 0}^{\Delta t \times k} \eta_{[I(t_k), T(t_k), SoC(t_k), SoH(t_k)]} \times I(t_k) \times \Delta t \tag{4}$$

Generally speaking, the definition domain of Coulombic efficiency, η , is continuous. It is impossible to obtain an accurate η for each point in the definition domain. Thus, we have to discretize

the definition domain into lattices with the same size. In the same lattice, the Coulombic efficiencies of these points are set to the same values. Thus:

$$SOC(t) \approx SOC(t_0) - \frac{1}{C_N} \times \sum_{t_k=\Delta t \times 0}^{\Delta t \times k} \eta_{[T^*(t_k), T^*(t_k), SOC^*(t_k), SOH^*(t_k)]} \times I(t_k) \times \Delta t \tag{5}$$

Having discretized the whole definition domain into lattices and calculated the whole capacity for points in the same lattice, we can number these lattices with “ L_1, L_2, \dots, L_n ” and calculate the SoC of battery with Equation (3),

$$SOC(t) \approx SOC(t_0) - \frac{1}{C_N} \times [\eta_{L_1} \times Q_{L_1} + \eta_{L_2} \times Q_{L_2} + \dots + \eta_{L_n} \times Q_{L_n}] \tag{6}$$

In fact, accurately determining these Coulombic efficiencies, η_{L_i} , is a hard thing. The relationship between the discharge capacity and the operating current/battery temperature/SoH is complicated and nonlinear. In the k^{th} cycle, the released capacity Q_k^* can be expressed like this:

$$Q_k^* \approx C_N \times (SOC(t_0) - SOC(t)) \approx \eta_{L_1} \times Q_{L_1,k} + \eta_{L_2} \times Q_{L_2,k} + \dots + \eta_{L_n} \times Q_{L_n,k} \tag{7}$$

where $Q_k^* = \eta \times Q_k + \epsilon_k$ where $\eta = \{\eta_{L_1}, \eta_{L_2}, \dots, \eta_{L_n}\}$ be the vector of Coulombic efficiency, $Q_k = \{Q_{L_1,k}, Q_{L_2,k}, \dots, Q_{L_n,k}\}$ be the accumulated capacities for lattices, ϵ_k be the error.

Having implemented K cycles, we can obtain the matrix:

$$\begin{cases} Q_1^* = \eta_{L_1} \times Q_{L_1,1} + \eta_{L_2} \times Q_{L_2,1} + \dots + \eta_{L_n} \times Q_{L_n,1} + \epsilon_1 \\ Q_2^* = \eta_{L_1} \times Q_{L_1,2} + \eta_{L_2} \times Q_{L_2,2} + \dots + \eta_{L_n} \times Q_{L_n,2} + \epsilon_2 \\ \dots \\ Q_K^* = \eta_{L_1} \times Q_{L_1,K} + \eta_{L_2} \times Q_{L_2,K} + \dots + \eta_{L_n} \times Q_{L_n,K} + \epsilon_K \end{cases} \tag{8}$$

There are many methods that can be used to estimate the unknown parameter η as long as $L_n \leq K$. In this paper, we estimate η with the least square method. The minimized sum of squares is:

$$S = \sum_{k=1}^K (Q_k^* - \eta \times Q_k)^2 = \sum_{k=1}^K (Q_k^* - \sum_{j=L_1}^{L_n} \eta_j \times Q_{j,k})^2, j = L_1, L_2, \dots, L_n \tag{9}$$

To solve the extreme-value problem, we can get:

$$\frac{\partial S}{\partial \eta_j} = 2 \sum_{k=1}^K (Q_k^* - \sum_{j=L_1}^{L_n} \eta_j \times Q_{j,k}) \times Q_{j,k} = 0, j = L_1, L_2, \dots, L_n \tag{10}$$

In this way, the Coulombic efficiency, η , can be calculated after $K(L_n = K)$ time running and it can be refreshed every time a charge/discharge process has been completed. In fact, the accumulated capacities of lattices are quite different. This can be observed in Figure 3, in which Figure 3a is the statistical capacity distribution of an EV-taxi in two-dimensional space, and Figure 3b is the statistical capacity distribution in the Urban Dynamometer Driving Schedule (UDDS) in one-dimensional space.

From both of them, we can see that most of these capacities converged in several special lattices, so discretizing the definition domain into lattices and calculating the SoC with the revised η for each accumulated capacity Q_{L_i} is a suitable way to estimate the SoC or available capacities for batteries.

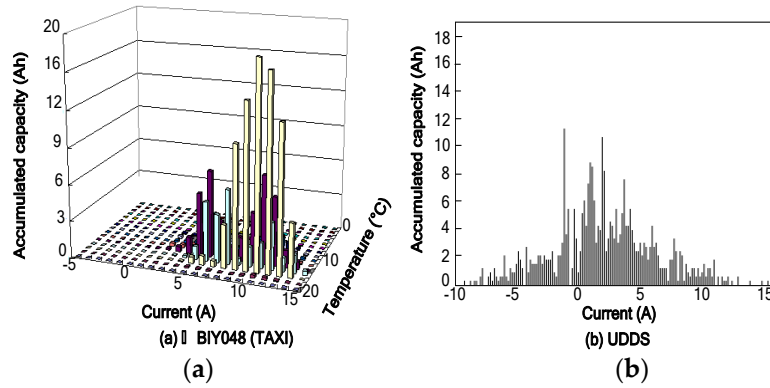


Figure 3. The capacity distributions in different driving cycles. (a) Jing BIY048 (TAXI); (b) UDDS.

3.1. The LC-Based Relative Coulomb Counting Method

Definition 5. (Bucket, b_j). Let the measured values of current, temperature, SoC and SoH, $I(t_k)$, $T(t_k)$, $SoC(t_k)$, and $SoH(t_k)$, be a data stream, the incoming stream is conceptually divided into buckets. Each bucket has $\Delta Q \times (1/\epsilon)$ Ah capacity and is labeled by $b_j = Q_k/(\Delta Q \times (1/\epsilon))$. (Q_k is the total accumulated capacity from time t_0 to t_k and ΔQ is unit capacity)

Definition 6. (Data structure, DS). DS is a set of entries, in the form $(I^*(t_k), T^*(t_k), SoC^*(t_k), SoH^*(t_k), Q, \Delta)$, where $I^*(t_k)$, $T^*(t_k)$, $SoC^*(t_k)$, $SoH^*(t_k)$ are the discretized values for $I(t_k)$, $T(t_k)$, $SoC(t_k)$, $SoH(t_k)$. Q is the accumulated capacity for entry $(I^*(t_k), T^*(t_k), SoC^*(t_k), SoH^*(t_k))$. Parameter t_k is the measurement time at the k^{th} time-step. Δ is the maximum possible error in Q .

Algorithm

- (1): Initializing DS. Clear the records in it. Initialize the error ϵ , support s and unit capacity ΔQ .
 - (2): Recording data. For every time interval t_k , read in the measured values for $I(t_k)$, $T(t_k)$, $SoC(t_k)$, $SoH(t_k)$ and discretize these measured values, $I^*(t_k) = INT(I(t_k))$, $T^*(t_k) = INT(T(t_k))$, $SoC^*(t_k) = INT(10 \times SoC(t_k))/10$, $SoH^*(t_k) = INT(10 \times SoH(t_k))/10$. Having done this, calculate the discharge/charge capacity for the discretized lattice, $Q(t_k) = I(t_k) \times (t_k - t_{k-1})$.
 - (3): Look up DS to see whether or not an entry, $(I^*(t_k), T^*(t_k), SoC^*(t_k), SoH^*(t_k), Q, \Delta)$, has existed. If there is any, update the entry by increasing the capacity for it ($Q = Q + Q(t_k)$). Otherwise, establish a new entry $(I^*(t_k), T^*(t_k), SoC^*(t_k), SoH^*(t_k), Q = Q(t_k), \Delta = \Delta Q \times (b_j - 1))$ for it.
 - (4): Does a bucket boundary arrive? Yes, go (5); No, go (2).
 - (5): Prune DS by deleting the entries in it and go (2). The rule for deletion is “for an entry $(I^*(t_k), T^*(t_k), SoC^*(t_k), SoH^*(t_k), Q, \Delta)$, if $Q + \Delta \leq \Delta Q \times b_j$, then delete it”.
-

Whenever a user asks for the capacity list of items with threshold s , the entries ($Q \geq (s - \epsilon) \times \Delta Q \times k$) will be outputted. Thus, with the obtained list (the entries ($Q < (s - \epsilon) \times \Delta Q \times k$) were seen as zero), the SoC can be calculated by:

$$SoC \approx SoC(t_0) - \frac{1}{C_N} \times [\eta_{L1} \times Q_{L1} + \eta_{L2} \times Q_{L2} + \dots + \eta_{Ln} \times Q_{Ln}] \quad (11)$$

3.2. Algorithm Analysis

Theorem 1: Let $((I^*(t_k), T^*(t_k), SoC^*(t_k), SoH^*(t_k)), Q, \Delta)$ be an entry in the data structure DS, $I^*(t_k)$, $T^*(t_k)$, $SoC^*(t_k)$, $SoH^*(t_k)$ are the discretized values for $I(t_k)$, $T(t_k)$, $SoC(t_k)$, $SoH(t_k)$ at time t_k , Q be the accumulated capacities of $(I^*(t_k), T^*(t_k), SoC^*(t_k), SoH^*(t_k))$, Δ be the maximum possible capacity error in Q , b_j be the label of a bucket, k be the discrete time-step, ϵ be the given error, s be the given support degree, ΔQ be the given unit capacity. Let $Q^{I^*(t_k), T^*(t_k), SoC^*(t_k), SoH^*(t_k)}$ be the true capacity for $(I^*(t_k), T^*(t_k), SoC^*(t_k), SoH^*(t_k))$. Then,

- (A) If $((I^*(t_k), T^*(t_k), SoC^*(t_k), SoH^*(t_k)), Q, \Delta)$ does not appear in DS, then $Q^{I^*(t_k), T^*(t_k), SoC^*(t_k), SoH^*(t_k)} \leq Q_k \times \epsilon$;
- (B) If $((I^*(t_k), T^*(t_k), SoC^*(t_k), SoH^*(t_k)), Q, \Delta)$ appears in DS, then $Q \leq Q^{I^*(t_k), T^*(t_k), SoC^*(t_k), SoH^*(t_k)} \leq Q + Q_k \times \epsilon$;
- (C) If (for every time interval $t_k, Q(t_k) > \Delta Q$) is true, then, with the given error ϵ , the algorithm computes the distribution synopsis using at most $\frac{1}{\epsilon} \log(Q_k \times \epsilon / \Delta Q)$ entries.

Proof: According to definition 5, we can get $b_j = Q_k / (\Delta Q \times (1/\epsilon))$.

For the first bucket ($b_j = 1$), an entry $((I^*(t_k), T^*(t_k), SoC^*(t_k), SoH^*(t_k)), Q, \Delta)$ is deleted only when the capacity of it, $Q \leq \Delta Q \times b_j$. Q is also the true capacity of $(I^*(t_k), T^*(t_k), SoC^*(t_k), SoH^*(t_k))$. Thus, $Q^{I^*(t_k), T^*(t_k), SoC^*(t_k), SoH^*(t_k)} \leq \Delta Q \times b_j = Q_k \times \epsilon$.

For an entry $((I^*(t_k), T^*(t_k), SoC^*(t_k), SoH^*(t_k)), Q, \Delta)$ that gets deleted in the other buckets ($b_j > 1$), which was inserted into the DS when bucket $b_j = \Delta / \Delta Q + 1$ was being processed, the capacity Q of it is the additional capacity after the insertion. Thus, the true capacity of $(I^*(t_k), T^*(t_k), SoC^*(t_k), SoH^*(t_k))$ in bucket b_j was no more than $Q + \Delta$. According to the deletion rule appeared in step (5), we can get $Q + \Delta \leq \Delta Q \times b_{current} = Q_k \times \epsilon$. Thus, conclusion (A) is true.

In the first bucket ($b_j = 1$), if the capacity of an entry $\Delta = 0$, then $Q = Q^{I^*(t_k), T^*(t_k), SoC^*(t_k), SoH^*(t_k)}$. In other buckets, entry $((I^*(t_k), T^*(t_k), SoC^*(t_k), SoH^*(t_k)), Q, \Delta)$ is deleted at most $\Delta / \Delta Q$ times. If an entry appeared in the current bucket $b_{current}$, the true capacity of it $Q^{I^*(t_k), T^*(t_k), SoC^*(t_k), SoH^*(t_k)}$ will no more than $Q + \Delta$. Since $\Delta \leq \Delta Q \times (b_{current} - 1) \leq Q_k \times \epsilon$, we can get $Q \leq Q^{I^*(t_k), T^*(t_k), SoC^*(t_k), SoH^*(t_k)} \leq Q + Q_k \times \epsilon$. Thus, conclusion (B) is true.

Let $b_{current}$ be the current bucket id, $j \in [1, b_{current}]$, e_j be the number of entries in data structure DS, whose bucket id is $(b_{current} - b_j + 1)$. Then, the accumulated capacities of these entries appeared in such a bucket $(b_{current} - b_j + 1)$ must be greater than $\Delta Q \times b_j$. Otherwise, it would have been removed. Let the size of the buckets is $\Delta Q \times (1/\epsilon)$, thus, we can get:

$$\sum_{j=1}^h \Delta Q \times j \times e_j \leq h \times \Delta Q \times (1/\epsilon) \text{ for } h = 1, 2, \dots, b_{current}$$

When $h = 1$, the inequality Equation (11) can be changed into $\sum_{j=1}^{h=1} \Delta Q \times j \times e_j \leq \Delta Q \times (1/\epsilon)$. After transformation, we can get:

$$\sum_{j=1}^{h=1} e_j \leq \sum_{j=1}^{h=1} \frac{1}{j \times \epsilon}$$

When $h = 2$, we can get:

$$\sum_{j=1}^{h=2} j e_j + \sum_{j=1}^{h=1} e_j \leq \frac{2}{\epsilon} + \sum_{j=1}^{h=1} \frac{1}{j \times \epsilon}$$

$$j \sum_{j=1}^{h=2} e_j \leq \sum_{j=1}^{h=2} \frac{2}{j \times \epsilon}$$

In this way, when $h = 1, 2, \dots, b_{current}$, we can get:

$$\sum_{j=1}^h j e_j + \sum_{j=1}^{h-1} e_j + \dots + \sum_{j=1}^{h-2} e_j + \sum_{j=1}^{h-1} e_j \leq h w + \sum_{j=1}^{h-1} \frac{w}{b_j} + \dots + \sum_{j=1}^{h-2} \frac{w}{b_j} + \sum_{j=1}^{h-1} \frac{w}{b_j}$$

$$h \cdot \sum_{j=1}^h e_j \leq h \cdot \frac{1}{\epsilon} + \sum_{j=1}^{h-1} \frac{(h-j)}{j \times \epsilon}$$

Since $|b_{current}| = \sum_{j=1}^{b_{current}} e_j$, we can get:

$$|b_{current}| \leq \sum_{j=1}^{b_{current}} \frac{1}{j \times \varepsilon} \leq \frac{1}{\varepsilon} \log b_{current} = \frac{1}{\varepsilon} \log\left(\varepsilon \cdot \frac{Q_k}{\Delta Q}\right)$$

Thus, conclusion (C) is true.

From conclusions (A)–(C), we can find that when the entries tend to uniformly distribute at random, the proposed algorithm can obtain the summary information of the accumulated current with very low space. At the same time, the statistical accuracy is guaranteed.

4. Experiments

The test bench, which consists of a thermal chamber for environment control, a host computer, a BaTe battery test system NBT BTS5200C4 and BeltControl 2.0 interface for programming the NBT BTS5200C4 is shown in Figure 4. The maximum voltage, maximum charge/discharge current, current control accuracy and voltage control accuracy of the NBT BTS5200C4 were 5.0 V, 200A, $\pm (0.1\%FD + 0.1\%RD)$ and $\pm (0.1\%FD + 0.1\%RD)$. In fact, the device can record the experimental data including temperature, current, voltage, accumulative amp-hours (Ah) and watt-hours (Wh). The host computer can collect the data through RS232/RS485 protocol. Four LFP cells (Battery-1, Battery-2, Battery-3 and Battery-4) were utilized to examine the accuracy of the proposed algorithm.



Figure 4. The battery test bench.

4.1. How to Reduce the Dimension of Coulombic Efficiency, η

Generally speaking, the Coulombic efficiency η is a function of current, temperature, SoC and SoH. From Equations (3) and (4) we can see that, to obtain an accurate value of SoC or available capacity, we have to discretize the definition domain of η into more lattices. This will lead to more expense. In fact, for an EV or HEV, the Coulombic efficiencies of the batteries are greatly affected by the fluctuations of discharge current and environmental temperature, slightly or slowly affected by SoC and SoH. In a short-term running, the change of SoH is very little. In the SoC range of 20%–100%, the Coulombic efficiency at the same temperature, SoH and charge/discharge current remains almost unchanged. This can be observed in Figure 2d. Thus, we can discretize the definition domain of η only in two-dimension space and initialize only several key Coulombic efficiencies in this space. The Coulombic efficiencies of other points can be calculated by the four key points nearby. This can be seen from Figure 5, in which the Coulombic efficiency of point X is calculated by comparing with the Coulombic efficiencies of four other key nearby points. With the given function, $z_p = a_0 + a_1x_p + a_2y_p + a_3x_p y_p$ and four nearest key points, A, B, C and D, the Coulombic efficiency of point X, η_x , can be easily calculated by solving the equation.

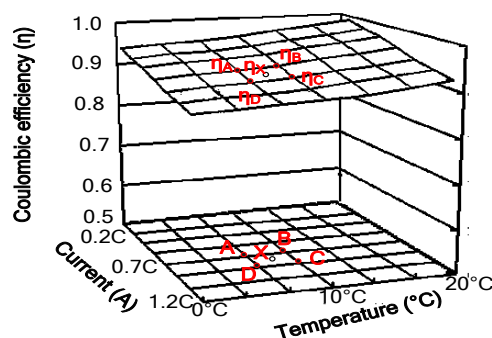


Figure 5. The Coulombic efficiencies of critical and non-critical points.

4.2. The Influences of Discharge Order and Frequency

From Equation (7) we can see that the proposed LC-based available capacity estimation method can calculate the accumulated capacities for lattices. However, the discharging order and frequency of these lattices cannot be recorded in the accumulation process. The discharging order and frequency are some other parameters which possibly influence the calculated available capacity. To make this point clear, several experiments were conducted and the results are shown below.

4.2.1. The Influences of Discharge Order

To examine the influence of discharge order on the obtained available capacity, three experiments were conducted on Battery-1. In Experiment-1, a total of two discharge procedures were carried out. The battery was firstly required to discharge at 8 A for 2 Ah and then discharged at 2 A until the voltage reaches the discharge threshold. This can be observed in Figure 6a, where the discharged capacity of battery-1 at 2 A is 4.001 Ah. In Experiment-2, the battery was firstly required to discharge at 2 A for 1 Ah, and then, discharge at 8 A for 2 Ah. Finally, it is discharged at 2 A until the voltage reaches the discharge threshold (2.5 V). This can be observed in Figure 6b. In Experiment-3, the battery was firstly required to discharge at 2 A for 4.001 Ah and then, discharged at 8 A for 0.222 Ah. After each of these experiments, the battery was required to rest for 1 h.

By comparing the three discharge experiments, we can find that without calculating the Coulombic efficiency, the total discharge capacities of the three experiments are not equal. The capacity difference between Experiment-1 and Experiment-2 is very small ($1.998 + 4.001 - 1.001 - 2.002 - 2.808 = 0.188$ Ah). The capacity difference between Experiment-1 and Experiment-3 is “ $1.998 + 4.001 - 4.001 - 0.222 = 1.776$ Ah”. This is very large for a low-capacity battery.

In fact, discharge order has no noticeable influence on the discharge capacity. The reason (why the discharged capacities, in Experiment-1 and Experiment-3, were so different?) lies in the insufficient power of the battery in Experiment-3. In Figure 6c, having discharged most of its capacity (4.001 Ah + 0.222 Ah), Battery-1 does not have sufficient power to maintain the discharging process. Thus, with the large discharge impedance, the voltage quickly falls to the cut off voltage (2.5 V). It is a fake fully-discharged-state and the SoC in Experiment-3 didn't reach zero. We can verify this by adding a resting stage (1 h) after each discharging experiment. Having done so, we found that the difference between the two open circuit voltages in Experiment-1 and Experiment-2, was very unimportant ($3.10 - 3.06 = 0.04$ V). In Experiment-1 and Experiment-3, the difference was very considerable ($3.10 - 3.23 = -0.13$ V). For a lithium-ion battery, the OCV-SoC charging or discharging curve is a flat one. A little difference in terminal voltage will lead to a huge gap in SoC. Thus, we can say that Battery-1 reaches similar states in Experiment-1 and Experiment-2. In Experiment-3, the its terminal status was distinct from the other cases, so it cannot be used to examine the influence of discharge order for the scheduled discharging procedure (8 A/2 Ah) was not completed.

From the experiments above, we can get the conclusion that, as long as the discharging power and cut off voltage were rightly controlled, discharge order has no obvious influence on discharge capacity.

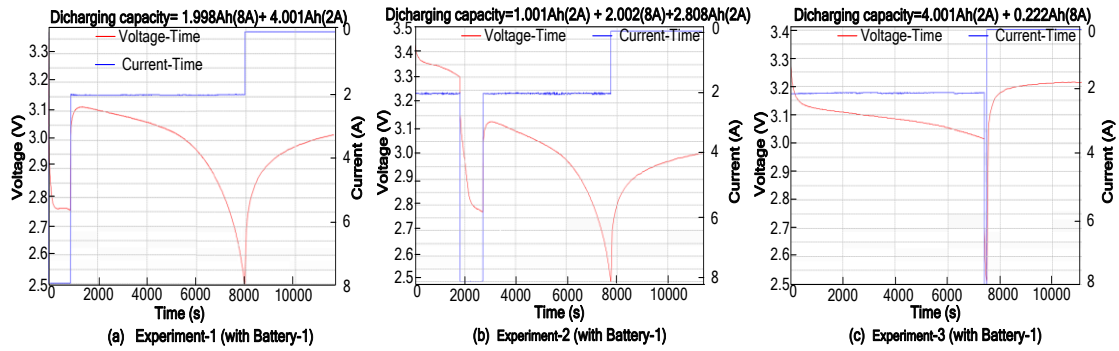


Figure 6. The influences of discharge order. (a) Experiment-1 (with Battery-1); (b) Experiment-2 (with Battery-1); (c) Experiment-3 (with Battery-1).

4.2.2. The Influences of Discharge Frequency

From Equations (3)–(7) and Figure 3, we can see that the accumulated capacities of the lattices can be achieved by the proposed LC-based SoC estimation method, but the frequencies of different charge/discharge operations cannot be recorded by the proposed algorithm.

To examine the low-frequency feature of the proposed algorithm, three discharge experiments were performed on Battery-2. All of these experiments include two kinds of discharge steps. In step-1, the discharge current is 8 A. In step-2, the discharge current is 2 A. In all of these experiments, both the discharge capacities in step-1/step-2 are 2 Ah. Having consumed the scheduled capacity for step-1 (2 Ah) and step-2 (2 Ah), discharge procedures keep discharging at a 2 A rate until the voltage threshold is reached. From Figure 7a–c, we can see that the total discharge capacities of the three experiments are 5.712 Ah, 5.597 Ah and 5.770 Ah. The differences between them are very small.

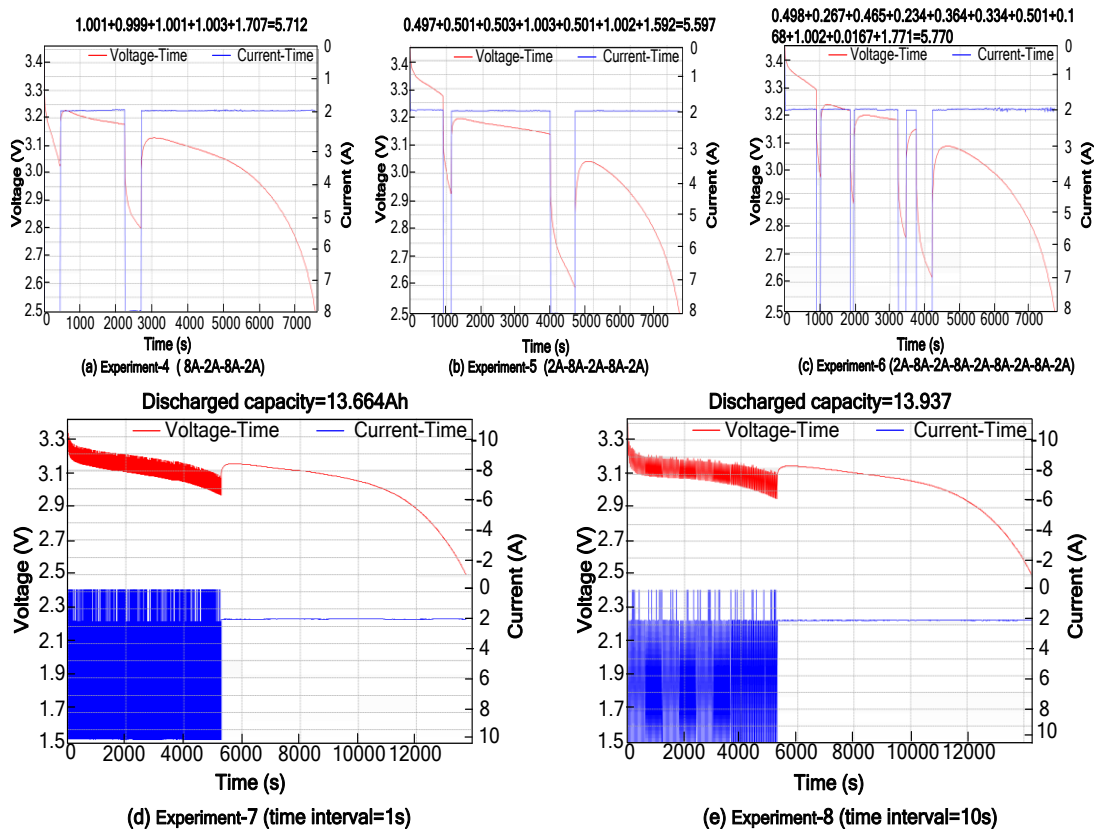


Figure 7. The discharge procedures with different discharging frequencies. (a) Experiment-4 (8A-2A-8A-2A); (b) Experiment-5 (2A-8A-2A-8A-2A); (c) Experiment-6 (2A-8A-2A-8A-2A-8A-2A-8A-2A); (d) Experiment-7 (time intervals = 1 s); (e) Experiment-8 (time intervals = 10 s).

To examine the high-frequency features of the proposed algorithm, we further implemented two high-frequency discharge experiments on Battery-3. Their discharge intervals are 1 s and 10 s. The scheduled capacities (C1 and C2) for discharge current-1 (10 A) and current-2 (2 A) in the two experiments are the same. Having consumed the accumulated capacities, C1 and C2, discharge procedures keep discharging at a 2 A rate until the discharge voltage threshold is reached. From Figure 7d–e, we can also find that the total discharge capacities of the two experiments are very similar. One is 13.664 Ah, the other is 13.937 Ah. Thus, we can say that the discharge capacity has no relation to discharge frequency.

4.3. Verification of the Proposed Estimation Method

Figure 8 illustrates the process of the verification experiment for the proposed LC-based estimation method. Two kinds of discharging cycles (UDDS and TAXI) were used for testing the proposed algorithm. Both experiments were performed at 10 °C. The current, voltage and operating time were examined every 0.1 s, 1 s, 2 s, 5 s, 10 s and 20 s. Before the examination point (E1/E2), the discharging process was conducted with the given driving cycles. After them, the battery was discharged with 2 A to the cut-off voltage. The discharge current is discretized into 10 lattices, and 10 Coulombic efficiency coefficients were initialized to 1. In fact, the charge/discharge capacity, obtained at different currents, can be transformed into an equivalent capacity at a constant current. In this section, the constant current is set to 2 A and the discharge Coulombic efficiency of 2 A, η_{2A} , is artificially set to 1. Thus, the equivalent discharged capacity (Q_j) for variable current j can be expressed by $Q_j = \eta_j Q_j / \eta_{2A}$, where Q_j is the accumulated capacity for current j , η_j is the Coulombic efficiency for current j . Thus, the estimated equivalent discharged capacity at the examined point E1, $Q_{i,(0-E1)}$, can be calculated by:

$$Q_{i,(0-E1)} = \eta_{0-2A} \times Q_{0-2A,i} + \eta_{2-4A} \times Q_{2-4A,i} + \dots + \eta_{18-20A} \times Q_{18-20,i}$$

After 10 discharging cycles, we obtained the equation set below:

$$\begin{cases} Q_{1,(0-E1)} = \eta_{L1,1} \times Q_{L1,1} + \eta_{L2,1} \times Q_{L2,1} + \dots + \eta_{L10,1} \times Q_{L10,1} \\ Q_{2,(0-E1)} = \eta_{L1,2} \times Q_{L1,2} + \eta_{L2,2} \times Q_{L2,2} + \dots + \eta_{L10,2} \times Q_{L10,2} \\ \dots \\ Q_{i,(0-E1)} = \eta_{L1,i} \times Q_{L1,i} + \eta_{L2,i} \times Q_{L2,i} + \dots + \eta_{L10,i} \times Q_{L10,i} \\ \dots \\ Q_{10,(0-E1)} = \eta_{L1,10} \times Q_{L1,10} + \eta_{L2,10} \times Q_{L2,10} + \dots + \eta_{L10,10} \times Q_{L10,10} \end{cases} \quad (14)$$

In both experiments, the available capacity C_N was defined as the discharged capacity of the battery at the discharging current 2 A. Thus, for each of the discharge cycle i , the true equivalent discharged capacity of it at the examination point E1, $Q_{i,(0-E1)}^*$, can be expressed by $Q_{i,(0-E1)}^* = C_N - Q_{i,(E1-END)}$. $Q_{i,(E1-END)}$ is the discharge capacity of the battery at 2 A, from time E1 to the end. In this way, equation set Equation (14) can be modified into Equation (15):

$$\begin{cases} C_N - Q_{1,(E1-END)} = \eta_{0-2A,1} \times Q_{0-2A,1} + \eta_{2-4A,1} \times Q_{2-4A,1} + \dots + \eta_{18-20A,1} \times Q_{18-20,1} + \varepsilon_1 \\ C_N - Q_{2,(E1-END)} = \eta_{0-2A,2} \times Q_{0-2A,2} + \eta_{2-4A,2} \times Q_{2-4A,2} + \dots + \eta_{18-20A,2} \times Q_{18-20,2} + \varepsilon_2 \\ \dots \\ C_N - Q_{i,(E1-END)} = \eta_{0-2A,i} \times Q_{0-2A,i} + \eta_{2-4A,i} \times Q_{2-4A,i} + \dots + \eta_{18-20A,i} \times Q_{18-20,i} + \varepsilon_i \\ \dots \\ C_N - Q_{10,(E1-END)}^* = \eta_{0-2A,10} \times Q_{0-2A,10} + \eta_{2-4A,10} \times Q_{2-4A,10} + \dots + \eta_{18-20A,10} \times Q_{18-20,10} + \varepsilon_{10} \end{cases} \quad (15)$$

Thus, if we initialize the Coulombic efficiency, $\eta = \{\eta_{L1}, \eta_{L2}, \dots, \eta_{Ln}\}$, with 1 in the first 10 equations, and accumulate the capacities for lattices in each discharge cycle. After running ten times, the accurate Coulombic efficiencies will be obtained with Equations (9) and (10), gradually.

In Figure 9, two kinds of Coulomb counting methods are shown. Charge/discharge cycles were carried out fifty times. We analyzed the performance of the two algorithms by comparing their relative mean errors. The red line indicates the relative mean errors between the real residual capacity and the estimated residual capacity. Real residual capacity is obtained by discharging the battery

with 2 A, from the examination point to the cut-off voltage. The estimated residual capacity is achieved with the proposed algorithm. The blue line is the relative mean error obtained with the traditional Coulomb counting method. It can be observed in Figure 10a,b that, on the one hand, with the increase of the time interval, the relative mean error gets larger and larger. On the other hand, the changing rates of the errors in the two algorithms are different. With the increasing time interval, the relative mean errors of the two algorithms get more and more similar.

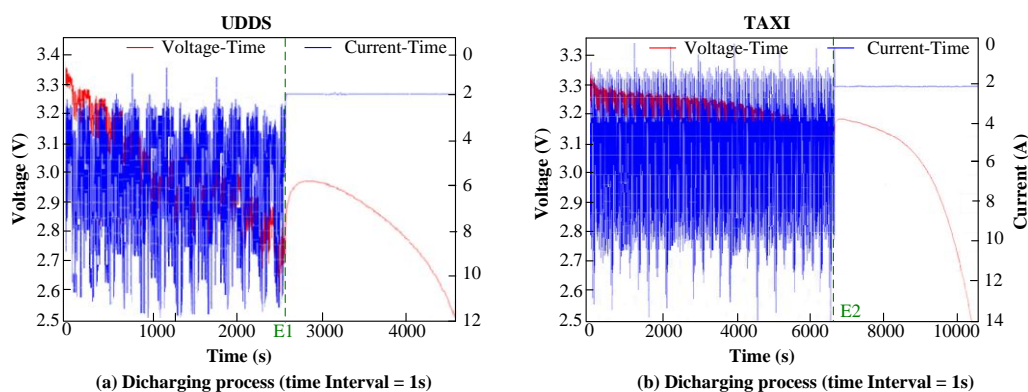


Figure 8. Two different discharging procedures (a) UDDS; (b) TAXI.

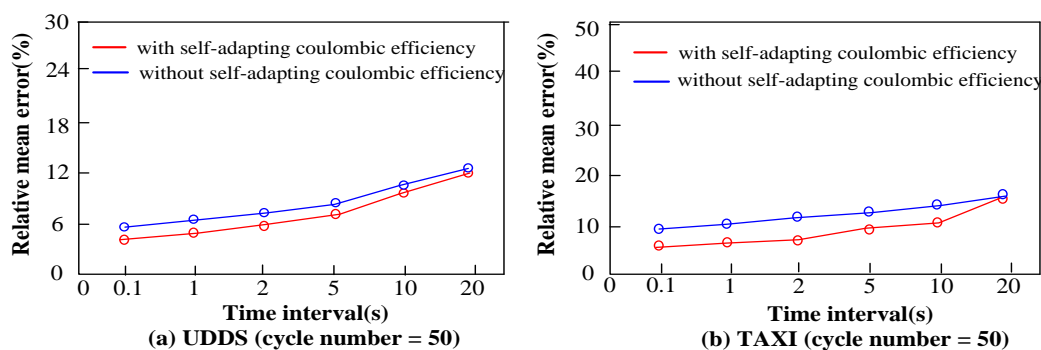


Figure 9. Relative mean errors of two different Coulomb counting methods. (a) UDDS; (b) TAXI.

4.4. The Influences of Measurement Interval

To further illustrate the impact of measurement time interval, we compared the estimation errors when the interval was set to 0.1 s, 1 s and 10 s. An actual discharging cycle, TAXI, was used to measure the errors. The experiment was carried out at 10 °C and the discharge current was discretized into 10 lattices. With the proposed method and the traditional method, we obtained the errors when the measurement interval was set to different values.

It can be observed in Figure 10a,b that, in the former ten driving cycles, the errors obtained with the two algorithms remain similar. However, after 10 implementations, the obtained results with the two algorithms are quite different. For the traditional Coulomb counting method, since no correction is carried out on the Coulombic efficiency, its estimation errors remain almost unchanged. For the proposed algorithm, by introducing the self-adapting Coulombic efficiency coefficient, η , the estimation error is reduced to nearly 5% and 6%, step by step. In the two methods, both the average error and the variation range of errors were enlarged when the measurement time interval was changed from 1 s to 10 s. It is quite conceivable that a larger measurement interval leads to a larger accumulated error, but accurate measurement means high computational cost and expensive devices.

In Figure 11, the accumulated capacities of ten current-intervals are shown. In Figure 11a, four different measuring procedures were performed. In both, the measurement intervals were set to 1s. In Figure 11b, four measurement intervals were set to 10 s. For both figures, the accumulated capacity, AC (measurement interval = 0.1 s), was seen as a basis of reference. Thus, with the comparison we

can find that the capacity difference between the measurement intervals of 0.1 s and 1 s is very little. This will lead to less error. On the contrary, the accumulated capacity difference between 0.1 s and 10 s is very large. Thus, it cannot be used to estimate the Coulombic efficiency coefficient, η , for an EV. In fact, “measurement interval = 0.1 s” is enough for an EV. Below it, no further benefit will be achieved and the profit coming from improving the measurement interval will be eroded by noise.

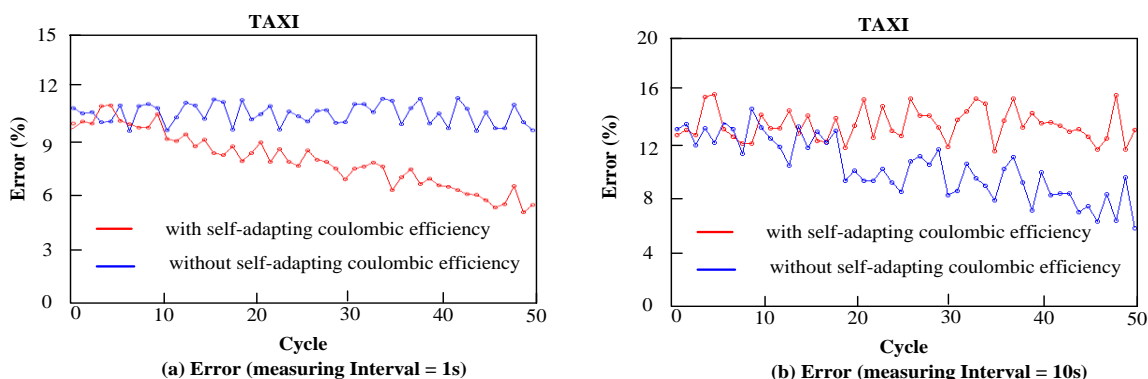


Figure 10. Estimation errors of two different Coulomb counting methods. (a) Measuring interval = 1 s; (b) Measuring interval = 10 s.

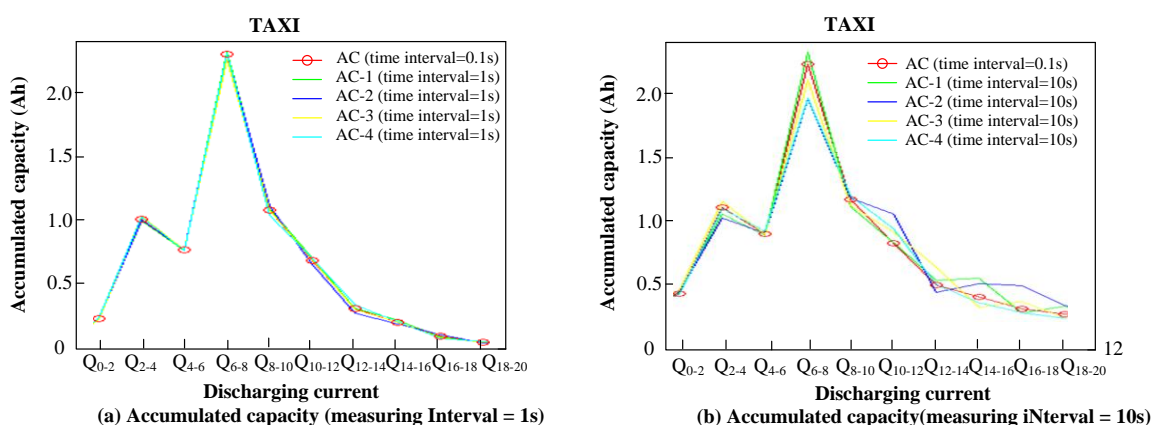


Figure 11. Accumulated capacities for different discharging currents. (a) Measuring interval = 1 s; (b) Measuring interval = 10 s.

4.5. The Influences of Noise

To further discuss the influence of the sensor noise, two kinds of noise were overlaid on the original current signals. The accumulated capacities for different lattices in the discharging cycle are shown in Figure 12, from which we can see that, when noise (−0.1 A–0.1 A) was overlaid on the original current signals, the distribution and total quantity of the accumulated charge obtained on the synthetic signals (red lines) were very similar to those in the original current signals (blue lines). When noise (0 A–0.2 A) was overlaid on the original signals, the distribution and the total accumulated charge on the synthetic signals (green lines) differed from those in the original signals (blue lines).

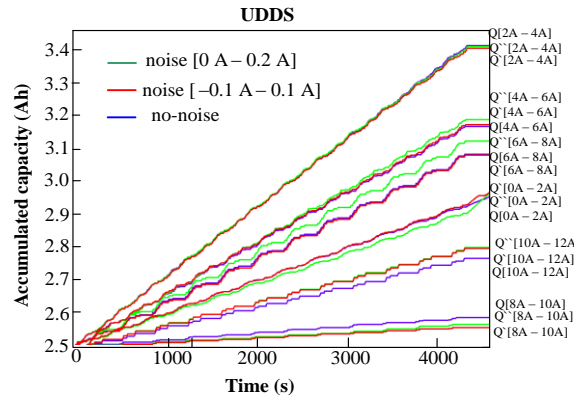


Figure 12. The accumulated capacities in different noisy environments.

Though the obtained current information was overlaid with the same noise signal, the relative errors obtained by the traditional Coulomb counting method and the proposed Coulomb counting method were quite different. This can be observed in Figure 13a,b, where three variation trends of the relative errors in different noise conditions were shown, respectively. By comparing Figure 13a and Figure 13b we can find that when noise (−0.1 A–0.1 A) was overlaid on the original current signals, the ranges (or trends) of the relative errors obtained with the two Coulomb counting methods remained unchanged. However, when noise (0 A–0.2 A) was overlaid on the original current signals, the relative errors obtained with the traditional Coulomb counting method increased, but the trend (or range) of the relative error obtained with the proposed Coulomb counting methods remained unchanged (in the latter 40 discharging cycles).

The answer resides in the equation set of Equation (15). When noise (0 A–0.2 A) was overlaid on the original current signals, all of the accumulated capacities for lattices L_n , $Q_{L_n,i}$ were increased. In the former 10 residual capacity calculation, the Coulombic efficiency, $\eta_{L_n,i}$ for each lattice cannot be revised, so the obtained errors will increase. However, after running 10 times (10 equations), the Coulombic efficiency, $\eta_{L_n,i'}$ begins to be revised dynamically. Although the Coulombic efficiencies, $\eta_{L_n,i'}$ were changed into distorted values as the polluted capacities, $Q_{L_n,i}$, were introduced, the ultimate estimation error is very small as the interaction effects exists.

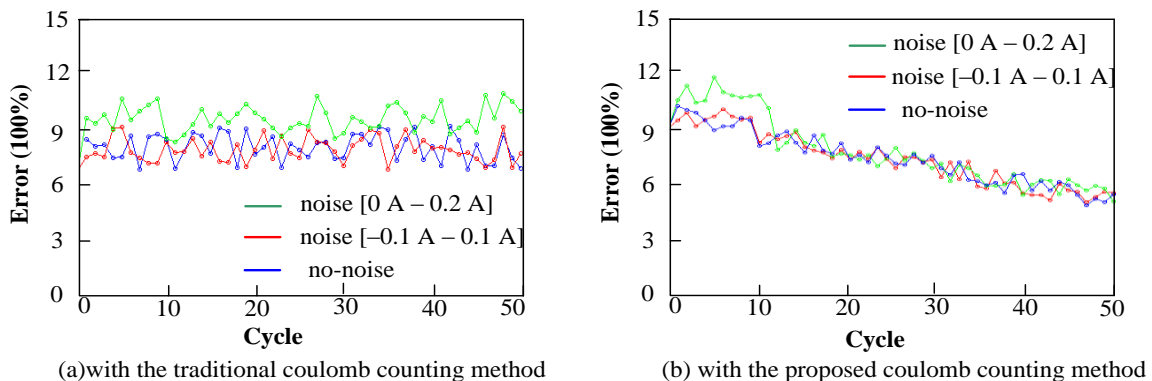


Figure 13. The relative errors in different noisy environments. (a) With the traditional coulomb counting method; (b) With the proposed coulomb counting method.

The changing specific process can be seen in Figure 14, where the values of two Coulombic efficiency, $\eta_{[4A-6A]}$ and $\eta_{[8A-10A]}$, were shown in Figure 14a,b. The corresponding accumulated capacities, $Q_{[4A-6A]}$ and $Q_{[8A-10A]}$ were presented in Figure 14c,d. With the intervention of the noise, the accumulated capacities, $Q_{[4A-6A]}$ and $Q_{[8A-10A]}$, increased in the total 50 driving cycles. However, the corresponding Coulombic efficiencies, $\eta_{[4A-6A]}$ and $\eta_{[8A-10A]}$, remain unchanged in the former 10 runs and decreased in the latter 40. Since no revision was carried out in the former 10 driving cycles (the

values of $\eta_{[4A-6A]}$ and $\eta_{[8A-10A]}$ kept unchanged), the relative errors obtained in the former 10 driving cycles were larger than that in the latter 40 driving cycles. Additionally, with the increasing noise (from [0A~0.1A] to [0.1A~0.2A]), the accumulated capacity was enlarged. The reverse movement of the Coulombic efficiency makes the final error decrease.

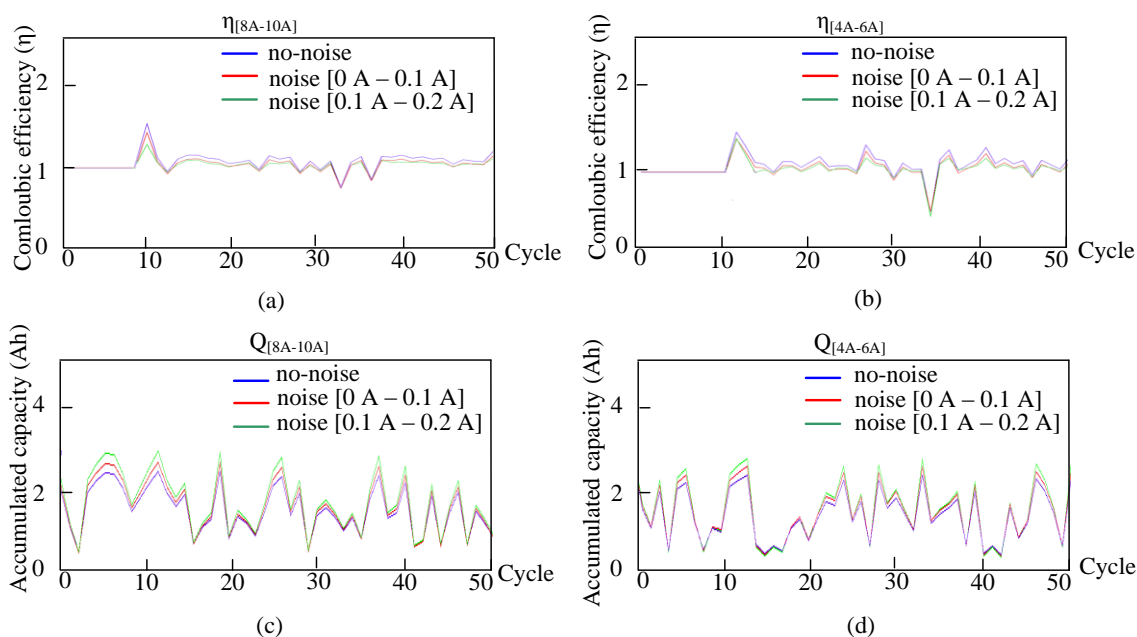


Figure 14. The relative errors in different noisy environments. (a) $\eta_{[8A-10A]}$; (b) $\eta_{[4A-6A]}$; (c) $Q_{[8A-10A]}$; (d) $Q_{[4A-6A]}$.

5. Conclusions

Estimating the residual capacity or state-of-charge for commercial batteries on-line without destroying them or interrupting the power supply, is a challenging task for battery management systems. In many traditional Ampere-hour integral methods, the SoC or residual capacity were calculated with an estimated Coulombic efficiency, η , the value of which remains unchanged in the whole charge/discharge cycle. However, its real value changes violently during the whole charge/discharge cycle and is determined by many factors, such as the charging/discharging current, temperature, SoC range and SoH.

In this manuscript, a novel lossy counting-based Coulomb counting method was proposed to deal with this problem. The comparative study and experimental results showed that the proposed algorithm has the capabilities of correcting the cumulative error (coming from measurement drift) and calculating the accumulated charges with more accurate Coulombic efficiencies. The advantages of the proposed method are:

- (1) The Coulombic losses can be corrected by the proposed lossy counting-based relative Coulomb counting method, and the Coulombic efficiency matrix can be revised with the statistical information and the least squares method, every time a charge/discharge cycle has been completed.
- (2) The cumulative error, coming from the current sensor, can be compensated by the distorted Coulombic efficiency matrix. It largely reduces the cost and complexity of the circuit and current sensor.
- (3) As a data stream mining technique is integrated into the estimation process, the requirements of large size of memory and computable hardware resource are reduced.
- (4) The proposed method for calibrating Coulombic efficiency coefficients is a universal algorithm. For different kinds of batteries, the control parameters should be adjusted appropriately.

Acknowledgments: We are grateful to the anonymous referees for their invaluable suggestions to improve the paper. This work was supported by National Natural Science Foundation of China (51375048), The Importation and Development of High-Caliber Talents Project of Beijing Municipal Institutions (CIT & TCD20130328).

Author Contributions: Li Zhao wrote the paper. Hong Zhang performed the experiments and proofread the paper text. Yong Chen had the overall scientific overview of the procedure and made the simulations.

Conflicts of Interest: The authors declare no conflict of interest.

References

1. Zhang, C.; Jiang, J.; Zhang, W. A novel data-driven fast capacity estimation of spent electric vehicle lithium-ion batteries. *Energies* **2014**, *7*, 8076–8094.
2. Tian, Y.; Xia, B.; Wang, M. Comparison study on two model-based adaptive algorithms for soc estimation of lithium-ion batteries in electric vehicles. *Energies* **2014**, *7*, 8446–8464.
3. Gao, J.; Zhang, Y.; He, H. A real-time joint estimator for model parameters and state of charge of lithium-ion batteries in electric vehicles. *Energies* **2015**, *8*, 8594–8612.
4. Swierczynski, M.; Stroe, D.; Stan, A.; Teodorescu, R. Lifetime and economic analyses of lithium-ion batteries for balancing wind power forecast error. *Int. J. Energy Res.* **2015**, *39*, 760–770.
5. Yuan, S.; Wu, H.; Ma, X.; Yin, C. Stability analysis for li-ion battery model parameters and state of charge estimation by measurement uncertainty consideration. *Energies* **2015**, *8*, 7729–7751.
6. Feng, F.; Lu, R.; Zhu, C. A combined state of charge estimation method for lithium-ion batteries used in a wide ambient temperature range. *Energies* **2014**, *7*, 3004–3032.
7. Zhu, G.; Wen, K.; Lv, W. Materials insights into low-temperature performances of lithium-ion batteries. *J. Power Sources* **2015**, *300*, 29–40.
8. Jin, Z.; Xie, K.; Hong, X.; Hu, Z. Capacity fading mechanism in lithium sulfur cells using poly(ethylene glycol)-borate ester as plasticizer for polymer electrolytes. *J. Power Sources* **2013**, *242*, 478–485.
9. Chen, K.; Li, X. Accurate determination of battery discharge characteristics—A comparison between two battery temperature control methods. *J. Power Sources* **2014**, *247*, 961–966.
10. Xing, Y.; He, W.; Pecht, M.; Tsui, K.L. State of charge estimation of lithium-ion batteries using the open-circuit voltage at various ambient temperatures. *Appl. Energy* **2014**, *113*, 106–115.
11. Zheng, Y.; Lu, L.; Han, X. LiFePO₄ battery pack capacity estimation for electric vehicles based on charging cell voltage curve transformation. *J. Power Sources* **2013**, *226*, 33–41.
12. Zhu, L.; Sun, Z.; Dai, H.; Wei, X. A novel modeling methodology of open circuit voltage hysteresis for LiFePO₄ batteries based on an adaptive discrete Preisach model. *Appl. Energy* **2015**, *155*, 91–109.
13. Gandolfo, D.; Brandão, A.; Patiño, D.; Molina, M. Dynamic model of lithium polymer battery—Load resistor method for electric parameters identification. *J. Energy Inst.* **2015**, *88*, 470–479.
14. He, H.; Qin, H.; Sun, X.; Shui, Y. Comparison study on the battery SoC estimation with EKF and UKF algorithms. *Energies* **2013**, *6*, 5088–5100.
15. Cho, S.; Jeong, H.; Han, C.; Jin, S.; Lim, J.H.; Oh, J. State-of-charge estimation for lithium-ion batteries under various operating conditions using an equivalent circuit model. *Comput. Chem. Eng.* **2012**, *41*, 1–9.
16. Gao, P.; Zhang, C.; Wen, G. Equivalent circuit model analysis on electrochemical impedance spectroscopy of lithium metalbatteries. *J. Power Sources* **2015**, *294*, 67–74.
17. Smekens, J.; Paulsen, J.; Yang, W. A modified multiphysics model for lithium-ion batteries with a Li_{0.5}Ni_{1/3}Mn_{1/3}Co_{1/3}O₂ electrode. *Electrochim. Acta* **2015**, *174*, 615–624.
18. Dong, G.; Zhang, X.; Zhang, C.; Chen, Z. A method for state of energy estimation of lithium-ion batteries based on neural network model. *Energy* **2015**, *90*, 879–888.
19. Xu, J.; Mi, C.C.; Cao, B.; Cao, J. A new method to estimate the state of charge of lithium-ion batteries based on the battery impedance model. *J. Power Sources* **2013**, *233*, 277–284.
20. Sepasi, S.; Ghorbani, R.; Liaw, B.Y. Inline state of health estimation of lithium-ion batteries using state of charge calculation. *J. Power Sources* **2015**, *299*, 246–254.
21. Zhang, C.; Li, K.; Pei, L.; Zhu, C. An integrated approach for real-time model-based state-of-charge estimation of lithium-ion batteries. *J. Power Sources* **2015**, *283*, 24–36.
22. Wang, H.; Zhang, X.; Ouyang, M. Energy consumption of electric vehicles based on real-world driving patterns: A case study of Beijing. *Appl. Energy* **2015**, *157*, 710–719.

23. Tang, X.; Wang, Y.; Chen, Z. A method for state-of-charge estimation of LiFePO₄ batteries based on a dual-circuit stateobserver. *J. Power Sources* **2015**, *296*, 23–29.
24. Li, F.; Sun, Y.Y.; Yao, Z.H. Enhanced initial coulombic efficiency of LiNiCoMnO₂ cathode materials with superior performance for lithium-ion batteries. *Electrochim. Acta* **2015**, *182*, 723–732.
25. Ng, K.S.; Moo, C.-S.; Chen, Y.-P.; Hsieh, Y.-C. Enhanced coulomb counting method for estimating state-of-charge and state-of-health of lithium-ion batteries. *Appl. Energy* **2009**, *86*, 1506–1511.
26. Mahdi, A.E.; Faggion, L. New displacement current sensor for contactless detection of bio-activity related signals. *Sens. Actuators A Phys.* **2015**, *222*, 176–183.
27. Feng, X.; Gooi, H.B.; Chen, S. Capacity fade-based energy management for lithium-ion batteries used in PV systems. *Electr. Power Syst. Res.* **2015**, *129*, 150–159.
28. Saeed, S.; Roose, L.R.; Matsuura, M.M. Extended kalman filter with a fuzzy method for accurate battery pack state of charge estimation. *Energies* **2015**, *8*, 5217–5233.
29. Ye, Y.; Shi, Y.; Cai, N.; Lee, J.; He, X. Electro-thermal modeling and experimental validation for lithium ion battery. *J. Power Sources* **2012**, *199*, 227–238.
30. Zhang, X.; Kong, X.; Li, G.; Li, J. Thermodynamic assessment of active cooling/heating methods for lithium-ion batteries of electric vehicles in extreme conditions. *Energy* **2014**, *64*, 1092–1101.
31. Ye, Y.; Shi, Y.; Tay, A.A.O. Electro-thermal cycle life model for lithium iron phosphate battery. *J. Power Sources* **2012**, *217*, 509–518.
32. Saw, L.; Ye, Y.; Tay, A. Electrochemical-thermal analysis of 18,650 Lithium Iron Phosphate cell. *Energy Convers. Manag.* **2013**, *75*, 162–174.
33. Sun, D.; Zhang, G.; Yang, S. Re-stream: Real-time and energy-efficient resource scheduling in big data stream computing environments. *Inf. Sci.* **2015**, *319*, 92–112.
34. Zhao, L.; Wang, L.; Xu, Q. Data stream classification with artificial endocrine system. *Appl. Intell.* **2012**, *37*, 390–404.
35. Motwani, R.; Manku, G.S. Approximate frequency counts over data streams. In Proceedings of the 28th International Conference on Very Large Data Bases (VLDB), Hong Kong, China, 20–23 August 2002; pp. 346–357.



© 2015 by the authors; licensee MDPI, Basel, Switzerland. This article is an open access article distributed under the terms and conditions of the Creative Commons by Attribution (CC-BY) license (<http://creativecommons.org/licenses/by/4.0/>).